The Astrophysical Journal, 954:40 (6pp), 2023 September 1 https://doi.org/10.3847/1538-4357/ace894

Striped Jets in Post–Neutron Star Merger Systems

Emma Kaufman[1], I. M. Christie, A. Lalakos[1], A. Tchekhovskoy[1], and D. Giannios[2]
[1] Center for Interdisciplinary Exploration & Research in Astrophysics (CIERA), Physics & Astronomy, Northwestern University, Evanston, IL 60208, USA
ekaufman@u.northwestern.edu, ichristi231@gmail.com
[2] Department of Physics and Astronomy, Purdue University, 525 Northwestern Avenue, West Lafayette, IN 47907, USA

Received 2022 December 12; revised 2023 July 13; accepted 2023 July 17; published 2023 August 22

Abstract

Models invoking magnetic reconnection as the particle acceleration mechanism within relativistic jets often adopt a gradual energy dissipation profile within the jet. However, such a profile has yet to be reproduced in first-principles simulations. Here we perform a suite of 3D general relativistic magnetohydrodynamic simulations of post–neutron star merger disks with an initially purely toroidal magnetic field. We explore the variations in both the microphysics (e.g., nuclear recombination, neutrino emission) and system parameters (e.g, disk mass). In all of our simulations, we find the formation of magnetically striped jets. The stripes result from the reversals in the poloidal magnetic flux polarity generated in the accretion disk. The simulations display large variations in the distributions of stripe duration, τ, and power, $\langle P_\Phi \rangle$. We find that more massive disks produce more powerful stripes, the most powerful of which reaches $\langle P_\Phi \rangle \sim 10^{49}$ erg s^{-1} at $\tau \sim 20$ ms. The power and variability that result from the magnetic reconnection of the stripes agree with those inferred in short-duration gamma-ray bursts. We find that the dissipation profile of the cumulative energy is roughly a power law in both radial distance, z, and τ, with a slope in the range of $\sim$1.7–3; more massive disks display larger slopes.

Unified Astronomy Thesaurus concepts: Jets (870); Gamma-ray bursts (629); Magnetohydrodynamical simulations (1966)

1. Introduction

Relativistic jets are ubiquitous in many black hole (BH) accreting systems, such as supermassive BHs in active galactic nuclei and core-collapse and neutron-star (NS) merger gamma-ray bursts (GRBs; long and short, respectively). They are powerful gamma-ray emitters that often display large variability in their emission. However, despite the detection of several thousand long GRBs and hundreds of short GRBs (for catalog, see Fong et al. 2015), the emission processes and mechanisms for particle acceleration responsible for the prompt emission remain elusive. In the former, we refer to the long-debated synchrotron (Katz 1994; Sari et al. 1996) versus photospheric (Goodman 1986; Thompson 1994; Mészáros & Rees 2000) origin of the prompt emission. In this work, we focus on the latter: the mechanism for particle acceleration within GRB jets.

Such a mechanism has to depend upon how the jets are launched. For hydrodynamic flows (for recent 3D simulations, see, e.g., Gottlieb et al. 2020), internal shocks and mixing can be generated while the jet breaks out of the surrounding medium, i.e., the stellar envelope for long GRBs and dynamical ejecta for short GRBs, at which point particles can be heated to mildly relativistic temperatures (Rees & Meszaros 1994; Lazzati & Begelman 2010). However, relativistic jets from BH systems have long been argued to be highly magnetized and magnetically driven (Blandford & Znajek 1977) and are, therefore, more susceptible to dissipating via magnetic reconnection rather than internal shocks (see Sironi et al. 2015). Magnetic reconnection is an efficient process for dissipating the jet's magnetic energy (Spruit et al. 2001; Drenkhahn & Spruit 2002) to particle acceleration and has been adopted in many recent studies for reproducing the prompt emission of GRBs (Giannios 2008; Beniamini & Granot 2016; Bégué et al. 2017; Beniamini & Giannios 2017).

This raises an important question: how is reconnection triggered within the jet? Recent 3D general relativistic magnetohydrodynamic (GRMHD) simulations show that magnetized jets can profusely dissipate their magnetic energy due to magnetic instabilities in both short (Gottlieb et al. 2022b) and long (Gottlieb et al. 2022a) GRB contexts. However, the instabilities and the associated reconnection tend to develop when the jets run into the ambient medium. An alternate mechanism is for the wound-up magnetic field lines in a jet to develop a "striped wind" configuration, in which their polarity flips over a characteristic timescale, generated by a large-scale poloidal (i.e, pointing in the R- and z-directions) dynamo within the surrounding BH accretion disk (e.g., magnetorotational instability, MRI; see Balbus & Hawley 1991). Although this striped jet scenario has been utilized in theoretical models (Drenkhahn & Spruit 2002; Drenkhahn 2002; Giannios & Uzdensky 2019), the quest to find it in simulations of GRB central engines and their jets has remained elusive. The requirement for large-scale poloidal magnetic flux in launching relativistic jets (Blandford & Znajek 1977) has often been satisfied in previous studies embedding GRB accretion disks with purely poloidal magnetic fields (Christie et al. 2019; Fernández et al. 2019). Doing so, however, allows for the accumulation of substantial poloidal flux on the BH to occur on short timescales, thus negating the effect of any small-scale loops of opposite polarity created under the dynamo. However, Christie et al. (2019) demonstrated for the first time, using 3D GRMHD simulations, that an initially toroidal magnetic field embedded within a post-NS merger remnant disk can generate large-scale poloidal magnetic flux of alternating polarity, launching tightly collimated

Table 1
Simulation Setup for Our Toroidal Postmerger Models.

Model Name	Total Resolution $N_r \times N_\theta \times N_\phi$	Duration, $t_{\max}$ (s)	Duration, $t_{\max}$ ($10^5\ r_g/c$)	Initial Torus Mass ($10^{-2}\ M_\odot$)
BT	$512 \times 256 \times 128$	4.3	2.9	3.3
BT-NR	$512 \times 256 \times 128$	0.67	0.45	3.3
BT-LD	$512 \times 256 \times 256$	0.52	0.35	10
BT-LDN	$512 \times 256 \times 256$	0.19	0.13	10

Note. Simulations BT and BT-LD include nuclear physics, while BT-NR neglects nuclear recombination, and BT-LDN neglects all nuclear physics.

relativistic striped jets. Liska et al. (2020) found that more radially extended accretion disks also lead to the accumulation of large-scale poloidal flux on the BH and the formation of relativistic jets, albeit without magnetic polarity flips (see Section 4 for comparison). More recently, Gottlieb et al. (2023a, 2023b) considered more realistic initial conditions in the aftermath of a BH–NS merger and a stronger initial toroidal magnetic field and found that this also leads to the production of jets; they did not discuss the development of the polarity flips. Hayashi et al. (2023) found magnetic polarity flips for both poloidal and toroidal initial conditions in numerical relativity simulations of BH–NS mergers.

These recent results trigger a series of important questions. Under what conditions are the striped jets produced? What are the properties of the magnetic flux reversals within the disk and jets? Assuming the magnetic polarity reversals between the stripes trigger reconnection events in the jets, what is the distribution of energy dissipation along the jets? Here we investigate these questions by performing 3D GRMHD simulations of post-NS merger remnant disks with initially purely toroidal magnetic fields and a variety of initial conditions. In Section 2, we discuss the numerical setup of our simulations. In Section 3, we discuss the properties of the magnetic flux reversals within the disk and jets. In Section 4, we conclude.

2. Numerical Setup

A detailed description of our simulation setup can be found in Christie et al. (2019; their BT model[3]) but will be briefly summarized here. We performed our postmerger simulations using `HARMPI` (Tchekhovskoy 2019),[4] an enhanced version of the serial open-source code `HARM` (Gammie et al. 2003; Noble et al. 2006), with the addition of several physical processes, including neutrino cooling and nuclear recombination processes (for more details, see Fernández et al. 2019). All simulations follow the setup of the BT model (Christie et al. 2019), namely, a BH with mass $M_{\rm BH} = 3\,M_\odot$ and dimensionless spin parameter $a = 0.8$ surrounded by a magnetized gas torus with an initial electron fraction $Y_e = 0.1$ (see Table 1). In addition to the BT model with a torus mass of $0.033\,M_\odot$, we consider three postmerger disks that have slight variations in their initial conditions (Table 1 gives model names and parameters), namely, (i) neglecting nuclear recombination with a torus mass of $0.033\,M_\odot$ (BT-NR model), (ii) a larger torus with a mass of $0.1\,M_\odot$ with the inclusion of all nuclear physics of the BT model (BT-LD model), and (iii) a larger torus with a mass of $0.1\,M_\odot$ and neglecting all nuclear physics (BT-LDN model[5]). All tori were embedded with a purely toroidal magnetic field with a plasma-β, i.e., ratio of gas to magnetic pressure, of 5, corresponding to a maximum magnetic field strength of $\sim 5 \times 10^{14}$ G within the disk for the BT and BT-NR models. For more massive tori, the magnetic field will likely be stronger. All simulations were performed beyond 0.1 s, allowing for run times comparable to the typical duration ($\lesssim$2s) of short GRBs.

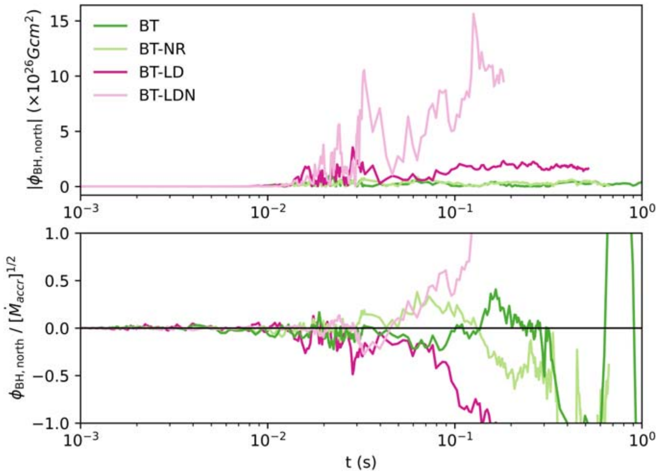

Figure 1. The dynamo-like action generates large-scale poloidal magnetic flux from a purely toroidal magnetic flux configuration and accretes it onto the BH (top panel, displaying the absolute value of magnetic flux in the northern hemisphere of the BH). Additionally, the dynamo-like action continuously generates flips in the magnetic flux (bottom panel, displaying magnetic flux normalized to the square root of the mass accretion rate). These flips in polarity result in the production of current sheets on the BH and hence striped jets. Interestingly, neglecting all nuclear physics and neutrino emission (BT-LDN model; see legend) results in stronger BH magnetic flux, as shown in the top panel, than all other models. However, the normalized flux is comparable across all models.

3. Results

Within the first ∼20 ms in all of our simulations, the mass accretion rate on the BH peaks (see Figure 1(a) in Christie et al. 2019) and launches subrelativistic outflows, which we refer to as disk winds. Interestingly, due to a dynamo-like action (Christie et al. 2019; Liska et al. 2020), these purely toroidal models result in the development of large-scale poloidal magnetic flux on the BH (the top panel of Figure 1 shows the time dependence of the absolute value of the magnetic flux through the BH). Our models also launch tightly collimated relativistic jets with opening angles $\theta_{\rm j} \lesssim 5°$ for the BT model. Christie et al. (2019) showed that jets in the BT model were not only intermittent but continuously flipped their magnetic polarity (i.e., resulted in striped jets), with current sheets separating the stripes of opposite polarity. This is illustrated in the bottom panel of Figure 1, which shows the northern component of the poloidal magnetic flux on the BH, defined as $\Phi_{\rm BH,north} = \int_{r=r_H} B^r dA$, normalized to the square root of the mass accretion rate on the BH. Here B^r is the radial component of the magnetic field, $r_H = r_g[1 + \sqrt{1 - a^2}]$ is the event horizon radius, $r_g = GM_{\rm BH}/c^2$ is the gravitational radius,

---

[3] For videos displaying the evolution of the BT model, see https://goo.gl/ct7Htx.

[4] https://github.com/atchekho/harmpi

[5] For videos displaying the evolution of the mass and current density in the BT-LDN model, see https://rb.gy/uojnpk.

$dA = \sqrt{-g}\, d\theta d\phi$ is the area element, and g is the determinant of the metric. Throughout, we adopt units such that $G = M_{\rm BH} = c = 1$.

This work aims to explore the consequences and robustness of striped jet formation in BH accretion simulations. It is not understood what mechanisms are responsible for the formation of the current sheets seen in the jets. In previous work, Christie et al. (2019) found that striped jets do not occur in their simulations with an initially poloidal magnetic field configuration. Similarly, Liska et al. (2020) did not find striped jets for simulations with an initially toroidal magnetic field, no nuclear microphysics, and a much larger initial torus than ours. We are interested in understanding how the disk mass affects the generation of stripes and whether physical processes such as nuclear recombination or neutrino physics are responsible for the striped jet generation.

3.1. Dynamo-like Behavior

All of our models have an initially purely toroidal field of nonnegligible strength. However, jets are launched by a poloidal magnetic field accreting onto the BH. In Figure 1, we plot the time dependence of the poloidal magnetic flux on the BH. Both the unnormalized (top panel) and normalized (bottom panel) magnetic flux grow over time, indicating that some process is converting the initially purely toroidal field to a large-scale poloidal field.

Dynamo processes have long been observed in shearing-box simulations of MRI (Brandenburg et al. 1995; Rincon 2019). Previous works such as Tomei et al. (2020, 2021) and Del Zanna et al. (2022) found that if they modified GRMHD equations of motion by including additional mean field dynamo terms in thick accretion disk simulations, they were able to convert a small seed field into a large-scale, ordered, poloidal magnetic field for initially toroidal and poloidal fields.

In our work, we do not modify GRMHD equations in any way, and we look for self-consistent formation of large-scale magnetic flux by magnetized turbulence. The exact process by which our simulations convert a toroidal field to a poloidal field is not yet clear. While understanding the processes responsible is beyond the scope of this work, future works will be looking in depth at this phenomenon (J. Jacquemin-Ide et al. 2023, in preparation). Throughout this work, we refer to these not-yet-understood processes as a “dynamo-like” action.

3.2. Properties of Magnetic Stripes

As discussed in Christie et al. (2019), the dynamo-like action within the disk continuously generates large-scale poloidal magnetic flux of alternating polarity. This can be seen for all models in Figure 1 via the northern component of the magnetic flux $\phi_{\rm BH,\ north}$ (top panel) and normalized to the square root of the mass accretion rate on the BH (bottom panel). At early times, $t \lesssim 10^{-2}$ s, the magnitude of $\phi_{\rm BH,\ north}$ slowly increases while fluctuating around zero, with the BT-LD model having slightly larger flux on the BH due to the higher mass accretion rate and therefore larger accumulation of magnetic flux on the BH. However, the BT-LDN model, which neglects all nuclear and neutrino physics, displays a large accumulation of a single polarity normalized flux at 0.05–0.2 s, beyond which field reversals cease.

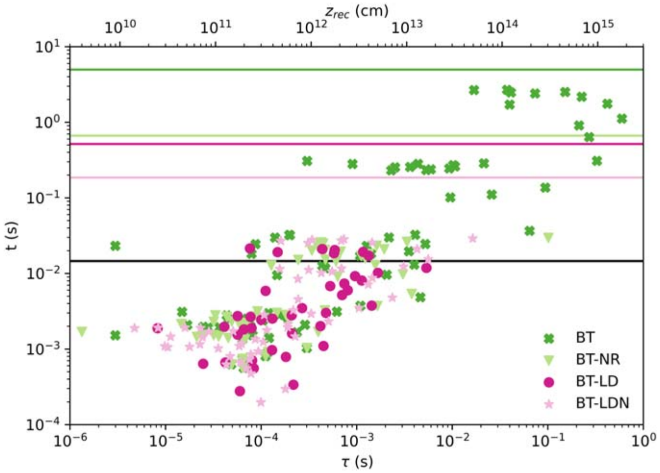

Figure 2. The duration τ of field reversals on the BH, determined from $\phi_{\rm BH,\ north}$ (see Figure 1) for all models considered (see legend), shows a general increase with increasing simulation time. For times $t \gtrsim 5 \times 10^{-2}$ s, our BT-LD, BT-LDN, and BT-NR models no longer exhibit flips in polarity up to the cessation of the simulation, denoted by the horizontal lines of the same color. Reversals produced at times $\gtrsim$0.015 s, i.e., times at which polar outflows begin to form (horizontal black line), will propagate and reconnect at various distances $z_{\rm rec}$ with the jet (see top axis). Here we use a fiducial value of $\Gamma_{\rm j} = 100$ for the jet Lorentz factor in computing $z_{\rm rec}$ (see Equation (1)).

To better understand the distribution of alternating polarity stripes seen in all of our models, we investigate the distribution of the time interval τ between the flips. Figure 2 shows the simulation time t as a function of stripe duration τ. At early times ($10^{-4}\ {\rm s} \lesssim t \lesssim 10^{-2}$ s), all models show a large spread in duration τ, which extends from $\tau \sim 10^{-5}$ to 10^{-2} s. Small duration flips can occur due to small-scale poloidal magnetic flux loops generated within the inner parts of the disk, which quickly accrete onto the BH. At late times, $t \gtrsim 0.05$ s, the magnitude of $\phi_{\rm BH,north}$ increases due to the increase in mass accretion rate and the accumulation of a single polarity flux on the BH, such that flips occur on longer timescales (i.e., $\tau \gtrsim 5 \times 10^{-3}$ s). Interestingly, by $t \sim 0.1$ s, the BT-LD, BT-LDN, and BT-NR models no longer exhibit polarity flips (see Figure 2) and instead have accumulated enough flux for a single polarity, as shown in the bottom panel of Figure 1. The BT model, however, continues to generate flux flips beyond 1 s, resulting in longer stripe durations of $\tau \gtrsim 0.1$ s.

The magnetic polarity flips can be associated with stripes propagating through the jet as long as they are produced at times after polar outflows begin to form ($t \sim 0.015$ s, denoted by the black line in Figure 2). If the polarity through the BH is fixed for time τ, the resulting jetted outflow (which flies out at nearly the speed of light c) maintains its polarity over the corresponding radial scale, $l = c\tau$, as measured in the BH frame. Each stripe propagating through the jet has a comoving width $\Gamma_{\rm j} l$, where $\Gamma_{\rm j}$ is the jet’s Lorentz factor. The stripes can ultimately reconnect within the jet at a radial distance as measured in the BH frame (Giannios & Uzdensky 2019),

$$z_{\rm rec} \approx \beta_{\rm rec}^{-1}\, \Gamma_{\rm j}^{2} l. \tag{1}$$

Here $\beta_{\rm rec} = v_{\rm rec}/c$ is the reconnection rate, which has been estimated via first-principles particle-in-cell simulations for varying plasma magnetizations and compositions (Sironi & Spitkovsky 2014; Guo et al. 2015; Sironi et al. 2016) and through analytical estimates (Lyubarsky 2005) as $\beta_{\rm rec} \approx 0.1$. The $\Gamma_{\rm j}^{2}$ factor in Equation (1) results from the combination of two relativistic effects: (i) the fact that the stripe width is a factor of Γ_j longer in the rest frame of the jet (where the magnetic

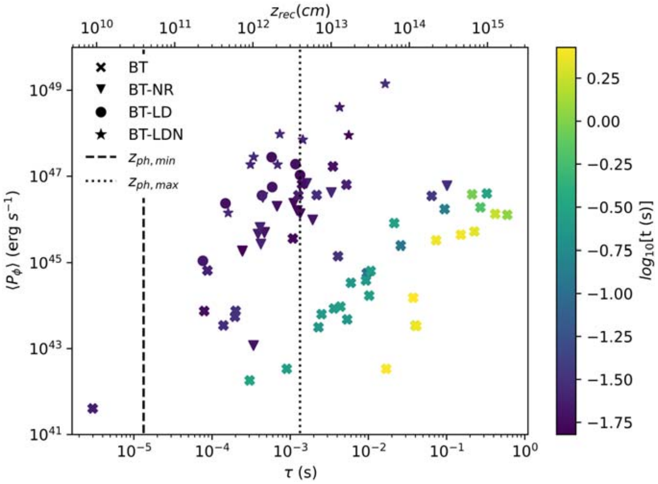

Figure 3. Time-averaged power $\langle P_\Phi \rangle$ (see Equation (2)) of each stripe propagating within the jet (see also Figure 2). Here $\langle P_\Phi \rangle$ is highly scattered for all models (see legend) as a function of τ, with the BT model displaying additional fluctuations as a function of simulation time (see color bar). The BT-LDN model, which neglects all nuclear physics, contains the stripes with the largest power. The black dashed (dotted) line shows the minimum (maximum) photospheric radius (see Equation (3)) using fiducial values of $\Gamma_\infty = 300$ and $\Gamma_j = 100$.

reconnection takes place) and (ii) the time dilation effect that prolongs, by another factor of Γ_j, how fast the reconnection takes place in the rest frame of the source. Adopting a typical GRB jet Lorentz factor of $\Gamma_{\rm j} = 100$, the stripes in our models can reconnect at distances of $z_{\rm rec} \sim 10^{10}$ cm -2×10^{15} cm $= 2.3 \times 10^4 r_g - 4.5 \times 10^9 r_g$. We show the distances at which the dissipation within the jet takes place along the top axis of Figure 2; we discuss this further in Section 3.3.

As each stripe reconnects within the jet, it can dissipate a fraction of its magnetic energy via relativistic magnetic reconnection, heating the plasma and accelerating particles. To determine the amount of dissipated energy, we can first calculate the time-averaged power within each stripe (Tchekhovskoy 2015),

$$\langle P_\Phi \rangle \approx \frac{\omega_H^2\, c}{96\, \pi^2\, r_g^2\, \tau} \int_{\rm stripe} dt\, |\Phi_{\rm BH}|^2, \tag{2}$$

where $\omega_H = a/(1 + \sqrt{1 - a^2})$. Our results for $\langle P_\Phi \rangle$ for all models as a function of τ and time t (indicated by the color bar) are shown in Figure 3.

As time increases beyond the time of initial jet formation, more magnetic flux accumulates on the BH and results in stripes of higher power. For a stripe of a given duration τ, the BT-LD and BT-LDN models generally contain stripes with larger power than the BT and BT-NR models, a direct result of the former models having a higher $\Phi_{\rm BH}$ at any given time.

3.3. Distribution of Energy Dissipation

The GRB jets can be opaque to electron scattering, i.e., if the optical depth is greater than unity, within the photospheric radius $z_{\rm ph}$ (Giannios 2012; Giannios & Uzdensky 2019):

$$z_{\rm ph} \approx 4 \times 10^{12}\, L_{52}\, \Gamma_{\infty,300}^{-1}\, \Gamma_{j,100}^{-2}\ {\rm cm}. \tag{3}$$

Here L is the jet's isotropic equivalent luminosity, Γ_∞ is the jet's asymptotic Lorentz factor, and we have adopted the notation $Q_x = Q/10^x$ in cgs units. Far within $z_{\rm ph}$, the radiated emission can be thermalized, leading to an apparent blackbody spectrum from the photosphere (Giannios & Spruit 2005). Dissipation occurring close to the photosphere, $z = z_{\rm ph}$, leads to Comptonization of photons by hot electrons, resulting in a high-energy power-law tail of the emission spectrum (Giannios 2006), while at $z \gg z_{\rm ph}$, the radiation is dominated by nonthermal synchrotron emission. The isotropic jet equivalent luminosity can be estimated as $L = L_{\rm j}/f_b$, where $L_{\rm j}$ is the intrinsic jet luminosity, and $f_b = 1 - \cos\theta_{\rm j}$ is the beaming factor assuming a jet opening angle of $\theta_{\rm j}$. Christie et al. (2019) showed that the peak of $L_{\rm j}$ and time-averaged opening angle, $\langle\theta_{\rm j}\rangle$, were highly dependent upon the initial magnetic field configuration within the disk, spanning ranges of $L_{\rm j} \sim 10^{50}$–10^{52} erg s^{-1} and $\langle\theta_{\rm j}\rangle \sim 4\overset{\circ}{.}6$–$13^\circ$. For the purely toroidal models presented here, we find similar jet peak powers in the range $L_{\rm j} \sim 10^{50}$–10^{51} erg s^{-1}. The corresponding isotropic equivalent luminosities are then estimated as $L \sim 10^{51}$–10^{53} erg s^{-1}. Adopting these and the fiducial values of $\Gamma_\infty \approx 300$ and $\Gamma_{\rm j} = 100$, the photospheric radius lies within $z_{\rm ph} \sim 4 \times 10^{10}$ cm -4×10^{12} cm[6] $= 8 \times 10^5 r_g - 8 \times 10^7\, r_g$.

In Figure 3, these characteristic $z_{\rm ph}$ values are overplotted with vertical black lines. Within the estimated lower bound, we find that only one stripe from the BT model, with $\tau \sim 3 \times 10^{-6}$ s, reconnects deep in the jet with a low $\langle P_\Phi \rangle$ of $\sim 7 \times 10^{41}$ erg s^{-1}. Stripes reconnecting within the upper estimated bound of $z_{\rm ph} \approx 4 \times 10^{12}$ cm can have durations up to ∼millisecond timescales. The average power of these stripes can span ∼5 orders of magnitude. Stripes reconnecting outside our upper estimates of $z_{\rm ph}$ display a large spread of durations, ranging from ∼millisecond timescales to ∼1 s, and luminosities. Although a majority of these stripes are produced within the BT model, we find that the most luminous stripes, as produced from the BT-LDN model with $\tau \sim 10$ ms and $\langle P_\Phi \rangle \sim 10^{49}$ erg s^{-1}, will reconnect outside the upper bound of $z_{\rm ph}$.

However, in reconnection, we are interested in not only the power contained within the stripes but also the amount of magnetic energy, estimated as $\langle E \rangle = \langle P_\Phi \rangle\, \tau$, available to be transferred to particle acceleration. More importantly, knowing the energy dissipation profile within the jet could assist in deciphering the origin of the prompt emission and the shape of the observed spectrum. In Figure 4, we plot the time-averaged energy $\langle E \rangle$ within each stripe (top panel) and the cumulative energy $\langle E \rangle_{\rm c}$ of all dissipating stripes (bottom panel) as a function of radial distance within the jet. In both panels, we see that the average energy per stripe is larger for the BT-LD and BT-LDN models. To obtain an estimate for the energy dissipation profile within the jet, we can perform a power-law fit to both $\langle E \rangle \propto \tau^\alpha$ and $\langle E \rangle_{\rm c} \propto \tau^\beta$. Here α (β) is estimated as ∼1.7 (1.8) for the BT model, ∼1.5 (1.7) for BT-NR, ∼2.5 (3) for BT-LD, and ∼2.2 (2.2) for BT-LDN. We note that $\alpha \approx \beta$ for all of our models, although we might have expected $\beta = \alpha + 1$ if $\langle E \rangle$ followed an exact power law without any scatter. This apparent inconsistency arises precisely due to the scatter; the value of α is dominated by the average power of the jet, whereas the value of β reflects the cumulative energetics of the jet and is dominated by the most energetic stripes (separated by quieter periods). Overall, β is the more useful measure of the jet dissipation energetics. For the cumulative energy $\langle E \rangle_c$ within the jet, we see that all of the energy ($\sim 5.8 \times 10^{44}$ erg)

---

[6] For a more detailed estimate of $z_{\rm ph}$ in the case of GRB 170817A, see Meng et al. (2018).

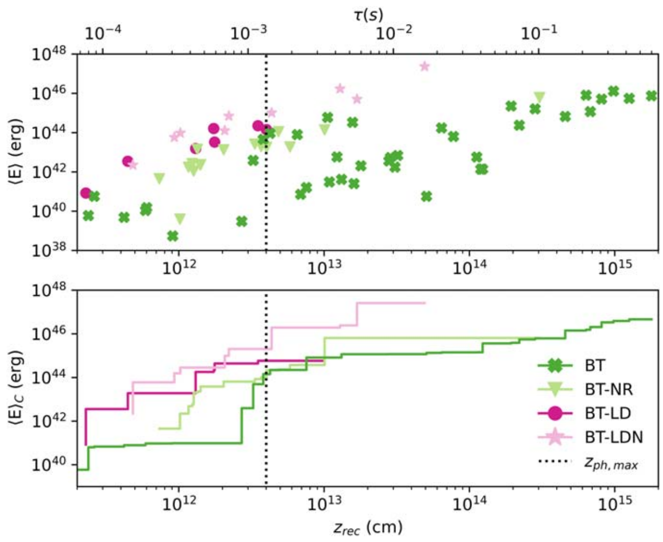

Figure 4. Time-averaged energy $\langle E \rangle$ per stripe (top panel) and cumulative energy $\langle E \rangle_{\rm c}$ of all stripes (bottom panel) as a function of radial distance z within the jet. The BT-LD model (see legend) dissipates all available energy within the estimated upper bound of the photospheric radius $z_{\rm ph,\, max}$ (vertical line), while the remaining models dissipate only a small fraction ($\lesssim 1.6\%$) of $\langle E \rangle_{\rm c}$. Here $\langle E \rangle$ ($\langle E \rangle_{\rm c}$) appears to constitute a power law as a function of radial distance and, equivalently, τ. Fitting each model, the slope can be estimated as ($\langle E \rangle$: 1.7, $\langle E \rangle_{\rm c}$: 1.8) for the BT model, ($\langle E \rangle$: 1.5, $\langle E \rangle_{\rm c}$: 1.7) for BT-NR, ($\langle E \rangle$: 2.5, $\langle E \rangle_{\rm c}$: 3) for the BT-LD model, and ($\langle E \rangle$: 2.2, $\langle E \rangle_{\rm c}$: 2.2) for the BT-LDN model.

for the BT-LD model will be dissipated at lower radii and within the estimated upper bound of the photospheric radius (see vertical line). The remaining three models, however, dissipate only a small fraction of the cumulative energy within $z_{\rm ph,\, max}$, with the BT model dissipating 1.4×10^{44} erg ($\sim$0.3%), 10^{44} erg ($\sim$1.6%) for the BT-NR model, and 2×10^{45} erg ($\sim$0.8%) for our BT-LDN model.

4. Discussion and Conclusion

Here we investigate the properties of naturally forming striped GRB jets as produced from 3D GRMHD simulations of post-NS merger disks. Beginning with a purely toroidal magnetic field and slight variations within the micro (i.e., nuclear recombination, neutrino emission) and macro (i.e., more massive disk) properties of the disk (see Table 1), we find that all models undergo a similar dynamo-like action within the disk, producing both large-scale poloidal magnetic flux (see Figure 1) and jets of alternating polarity. In addition to finding that more massive disks produce stripes of larger power (Figure 3), they accumulate larger amounts of a single polarity magnetic flux on the BH, resulting in the cessation of striped jets. Although the distributions in the magnetic stripe duration τ (Figure 2), power $\langle P_\Phi \rangle$ (Figure 3), and energy $\langle E \rangle$ (Figure 4) vary between all models, the robustness of the striped jet production signifies that it may be an inherent result of toroidally embedded compact disks and is less governed by microphysical details.

Here we used flux through the BH as proxy for the jet power. For stripes with $\tau > 10^{-4}$ s, this is a good approximation, but for shorter-duration flips with $\tau \sim 10^{-5}$ s, this is not as good an approximation, as the flips may not result in active jet phases. That being said, a large portion of the short-duration stripes occurring before the formation of the jet and those that occur after reconnecting within the photosphere are not observable.

The power displayed within short GRB jets is highly variable, ranging on timescales from submillisecond to $\sim$1 s (observed in both simulations and observations; Abbott et al. 2017a, 2017b; Christie et al. 2019; Gottlieb et al. 2020, 2022b). The dissipation of our observed stripes at a radial distance of $z_{\rm rec}$ within the jet corresponds to an observed variability on timescales of $t_v \simeq z_{\rm rec} / (\Gamma_j^2 c) \sim \tau / \beta_{\rm rec}$. Therefore, the most powerful stripes from our models, with τ ranging from $\sim$0.5 to $\sim$50 ms (see Figure 3), will display an observed variability ranging from $\sim$5 ms to $\sim$0.5 s, consistent with observations. As compared with former theoretical models of striped jets, the energy dissipation profile found here is distinctly different. Some models (Spruit et al. 2001; Drenkhahn & Spruit 2002; Drenkhahn 2002) calculate the energy dissipation profile assuming that the stripes are injected with a unique, characteristic timescale. These studies included the bulk acceleration profile for the jet, whereas we assumed a constant Lorentz factor in the dissipation region. On the other hand, Giannios & Uzdensky (2019) assumed an extended profile for the distribution of stripe length scales within the jet, finding a shallow cumulative energy profile $\langle E \rangle_{\rm c} \propto z^{1/3}$ up to a critical dissipation distance after which $\langle E \rangle_{\rm c}$ saturates at its asymptotic value. Moreover, they effectively associated the dominant stripe duration with timescales related to the inner edges of the disk, as might be expected in an extended, quasi-steady disk. Here, however, our disks are finite, narrow, and expand radially, thereby introducing stripes of progressively longer duration within the jet. Our simulations point to having more magnetic flux associated with the expanding outer edge of the disk and, therefore, with progressively longer timescales. Moreover, we calculate the jet dissipation profile assuming a fiducial value for the jet Lorentz factor, $\Gamma_{\rm j} = 100$. This assumption has a strong effect on whether the dissipation in the jet takes place at large or small Thomson optical depths. For instance, for slower jets (e.g., $\Gamma_{\rm j} \sim 30$), the distance, $z_{\rm rec}$, at which reconnection occurs (Equation (1)) decreases with increasing photospheric radius, $z_{\rm ph}$ (Equation (3)), resulting in the majority of the stripes in all of our models dissipating within $r_{\rm ph}$.

Our postmerger disk simulation results differ from those for radially extended disks of Liska et al. (2020), although both kinds of disks feature initially toroidal magnetic fields. Namely, Liska et al. (2020) found that although field reversals similarly occur within the disk, most of the generated poloidal magnetic flux loops are ejected as outflows from the disk; this results in a single magnetic loop dominating both the jet energetics and magnetic flux polarity. Christie et al. (2019) argued that these differences were due to (i) the smaller postmerger disks being more tightly bound and less conducive to outflows and/or (ii) neutrino cooling producing even more tightly bound disks. We show that striped jets persist, albeit exhibiting different distributions in τ and $\langle P_\Phi \rangle$, across a range of microphysics (e.g., with versus without neutrino cooling), system properties (e.g., different merger remnant disk masses), and simulation numerical resolutions (see Table 1). However, we note that the three new models presented here in comparison to Christie et al. (2019), namely, BT-NR, BT-LD, and BT-LDN, differ from the base BT model in accumulating sufficient magnetic flux by $t \sim 0.1$ s (see Figure 1) such that the stripes are no longer produced within the jet at later times. It is useful to benchmark these results with future studies that include, in the context of postmerger disks, more realistic microphysics and initial conditions (e.g., neutrino transport, realistic equation of state, more realistic postmerger initial conditions, and the inclusion of dynamical ejecta; see Foucart et al. 2014, 2019; Miller et al. 2019). Additionally, it is unclear how the initial magnetic field strength affects these results. Future work should vary the plasma-β in order to determine if the field strength affects the generation of stripes and the power they release.

Acknowledgments

We thank the anonymous referee for constructive feedback, which improved the clarity of this manuscript. E.K. thanks Jonatan Jacquemin, Evan Anders, and Daniel Lecoanet for their supportive conversations. E.K. acknowledges support by the National Science Foundation under grant No. AST-1757792, a Research Experiences for Undergraduates (REU) grant award. I.M.C. acknowledges support from Fermi Guest Investigation grants 80NSSC18K1745 and 80NSSC20K0213. A.T. was supported by Fermi Cycle 14 Guest Investigator program 80NSSC22K0031, NASA grants 80NSSC18K0565 and 80NSSC21K1746, and NSF grants AST-2107839, AST-1815304, AST-2009884, AST-1911080, OAC-2031997, and AST-2206471. A.T. was partly supported by NSF-BSF grant 2020747. D.G. acknowledges support from NSF AST-2107802 and AST-2107806 grants. This research used resources of the National Energy Research Scientific Computing Center, a DOE Office of Science User Facility supported by the Office of Science of the U.S. Department of Energy under contract No. DE-AC02-05CH11231 using NERSC award NP-ERCAP0020543. The software used in this work was developed in part by the DOE NNSA-ASC OASCR Flash Center at the University of Chicago. Computations were performed at Carver, Hopper, and Edison (repositories m1186, m2058, m2401, and the scavenger queue).

ORCID iDs

Emma Kaufman https://orcid.org/0000-0002-7236-284X
A. Lalakos https://orcid.org/0000-0002-6883-6520

References

Abbott, B. P., Abbott, R., Abbott, T. D., et al. 2017a, ApJL, 848, L13
Abbott, B. P., Abbott, R., Abbott, T. D., et al. 2017b, ApJL, 848, L12
Balbus, S. A., & Hawley, J. F. 1991, ApJ, 376, 214
Bégué, D., Pe'er, A., & Lyubarsky, Y. 2017, MNRAS, 467, 2594
Beniamini, P., & Giannios, D. 2017, MNRAS, 468, 3202
Beniamini, P., & Granot, J. 2016, MNRAS, 459, 3635
Blandford, R. D., & Znajek, R. L. 1977, MNRAS, 179, 433
Brandenburg, A., Nordlund, A., Stein, R. F., & Torkelsson, U. 1995, ApJ, 446, 741
Christie, I. M., Lalakos, A., Tchekhovskoy, A., et al. 2019, MNRAS, 490, 4811
Del Zanna, L., Tomei, N., Franceschetti, K., Bugli, M., & Bucciantini, N. 2022, Fluids, 7, 87
Drenkhahn, G. 2002, A&A, 387, 714
Drenkhahn, G., & Spruit, H. C. 2002, A&A, 391, 1141
Fernández, R., Tchekhovskoy, A., Quataert, E., Foucart, F., & Kasen, D. 2019, MNRAS, 482, 3373
Fong, W., Berger, E., Margutti, R., & Zauderer, B. A. 2015, ApJ, 815, 102
Foucart, F., Deaton, M. B., Duez, M. D., et al. 2014, PhRvD, 90, 024026
Foucart, F., Duez, M., Gudinas, A., et al. 2019, PhRvD, 100, 104048
Gammie, C. F., McKinney, J. C., & Tóth, G. 2003, ApJ, 589, 444
Giannios, D. 2006, A&A, 457, 763
Giannios, D. 2008, A&A, 480, 305
Giannios, D. 2012, MNRAS, 422, 3092
Giannios, D., & Spruit, H. C. 2005, A&A, 430, 1
Giannios, D., & Uzdensky, D. A. 2019, MNRAS, 484, 1378
Goodman, J. 1986, ApJL, 308, L47
Gottlieb, O., Issa, D., Jacquemin-Ide, J., et al. 2023a, arXiv:2306.14947
Gottlieb, O., Issa, D., Jacquemin-Ide, J., et al. 2023b, arXiv:2306.14946
Gottlieb, O., Liska, M., Tchekhovskoy, A., et al. 2022a, ApJL, 933, L9
Gottlieb, O., Moseley, S., Ramirez-Aguilar, T., et al. 2022b, ApJL, 933, L2
Gottlieb, O., Nakar, E., & Bromberg, O. 2020, MNRAS, 500, 3511
Guo, F., Liu, Y.-H., Daughton, W., & Li, H. 2015, ApJ, 806, 167
Hayashi, K., Kiuchi, K., Kyutoku, K., Sekiguchi, Y., & Shibata, M. 2023, PhRvD, 107, 123001
Katz, J. I. 1994, ApJL, 432, L107
Lazzati, D., & Begelman, M. C. 2010, ApJ, 725, 1137
Liska, M., Tchekhovskoy, A., & Quataert, E. 2020, MNRAS, 494, 3656
Lyubarsky, Y. E. 2005, MNRAS, 358, 113
Meng, Y.-Z., Geng, J.-J., Zhang, B.-B., et al. 2018, ApJ, 860, 72
Mészáros, P., & Rees, M. J. 2000, ApJ, 530, 292
Miller, J. M., Ryan, B. R., Dolence, J. C., et al. 2019, PhRvD, 100, 023008
Noble, S. C., Gammie, C. F., McKinney, J. C., & Del Zanna, L. 2006, ApJ, 641, 626
Rees, M. J., & Meszaros, P. 1994, ApJL, 430, L93
Rincon, F. 2019, JPlPh, 85, 205850401
Sari, R., Narayan, R., & Piran, T. 1996, ApJ, 473, 204
Sironi, L., Giannios, D., & Petropoulou, M. 2016, MNRAS, 462, 48
Sironi, L., Petropoulou, M., & Giannios, D. 2015, MNRAS, 450, 183
Sironi, L., & Spitkovsky, A. 2014, ApJL, 783, L21
Spruit, H. C., Daigne, F., & Drenkhahn, G. 2001, A&A, 369, 694
Tchekhovskoy, A. 2015, in The Formation and Disruption of Black Hole Jets, ed. I. Contopoulos, D. Gabuzda, & N. Kylafis (Cham: Springer), 45
TchekhovskoyA. (2019) HARMPI: 3D massively parallel general relativictic MHD code, Astrophysics Source Code Libraryascl:1912.014
Thompson, C. 1994, MNRAS, 270, 480
Tomei, N., Del Zanna, L., Bugli, M., & Bucciantini, N. 2020, MNRAS, 491, 2346
Tomei, N., Del Zanna, L., Bugli, M., & Bucciantini, N. 2021, Univ, 7, 259